Journal of Materials Chemistry A

PAPER

View Article Online
View Journal | View Issue

Cite this: J. Mater. Chem. A, 2018, 6, 11941

Flow-induced voltage generation by driving imidazolium-based ionic liquids over a graphene nano-channel†

Yongji Guan, [a] Qunfeng Shao,[c] Wenqiong Chen, [a] Jiao Zhang, [a] Xiaoping Zhang *[a] and Youquan Deng *[b]

Inspired by the interesting phenomenon that biological systems have the inherent skill to generate significant bioelectricity when the salt content in fluids flows over highly selective ion channels on cell membranes, in this study, the flow-induced voltage is investigated by driving the pure bulk room-temperature ionic liquid (RTIL) 1-ethyl-3-methylimidazolium tetrafluoroborate ([Emim][BF_4]) flowing over a graphene nano-channel consisting of two parallel single-layered graphene sheets using molecular dynamics simulation for the first time. Considering the combined effect of cations and anions in the adsorbed layer on the free charge carriers of the graphene surfaces (the interactions are 12.0 and 7.0 kJ mol^{-1} per cation/anion and graphene, respectively) and the characteristic of Coulomb's law, we have developed an advanced equation that can effectively and accurately calculate the flow-induced voltage of RTIL and graphene nano-channel system on the nano-scale. A maximum flow-induced voltage of 2.3 μV is obtained from this nano-scaled system because the free charge carrier on the graphene channel surfaces is dragged along the pure bulk RTIL's direction of movement. A saturation of the flow-induced voltage with increased flow velocity is observed, and this saturation can be attributed to the balance between the external driving force and viscous resistance arising from the internal RTIL and graphene nano-channel. Further analysis shows that the flow-induced voltages gradually increase towards saturation from 1.9 to 2.1 μV or decrease from 2.3 to 2.1 μV when the distance between the two parallel single-layered graphene or the area of single-layered graphene of the nano-channel increases from 1 to 5 nm or from 1 to 25 nm^2, respectively. Additionally, the influence of the system temperature (viscosity) and average flow velocity on the flow-induced voltage is investigated.

Received 21st March 2018
Accepted 24th May 2018

DOI: 10.1039/c8ta02629g

rsc.li/materials-a

1 Introduction

The potential applications of flow-induced voltage in nano-scaled self-powered devices as nano-electromechanical systems (NEMSs) have attracted widespread attention of researchers.[1–4] In 2009, Zhao and coworkers[2] first employed the structure of water-filled single-walled carbon nano-tubes (SWCNTs) to investigate the generation of flow-induced voltage using the mutual iterative method of density functional theory (DFT) and molecular dynamics (MD) simulation. A peak flow-induced voltage of 17.2 mV was obtained from water flowing on SWCNT with a diameter of 0.814 nm and length of 1.23 nm. The main mechanism of flow-induced voltage generation is attributed to charge redistribution in a SWCNT caused by interactions between the water dipole chains and charge carriers in a tube. Chen and Xu[3] explored the flow-induced voltage through the flow of 0.9 M hydrochloric acid (HCl)–water solution through a SWCNT with a diameter of 2.712 nm and length of 10.7 nm at room temperature using MD simulation. According to an equation used to calculate the flow-induced voltage developed by Ueba and coworkers[5] and only taking into account the effect of anions (Cl^- ions) on the flow-induced voltage, a flow-induced voltage of ~2 μV was obtained because the Cl^- ions showed a stick-slip motion near the wall owing to their strong interaction with carbon atoms and adjacent water molecules. Since nano-confined liquids exhibit an unexpectedly fast flow velocity, which benefits the induced voltage generation,[6,7] Koratkar *et al.*[4] have confined the 0.6 M HCl solution into the graphene nano-channel consisting of two parallel single-layered graphene sheets (4.26 × 2.46 nm^2) and obtained a flow-induced voltage of ~2.5 μV by driving the 0.6 M

[a]Institute of Optoelectronics and Electromagnetic Information, School of Information Science and Engineering, Lanzhou University, Lanzhou, 730000, People's Republic of China. E-mail: zxp@lzu.edu.cn

[b]Centre for Green Chemistry and Catalysis, Lanzhou Institute of Chemical Physics, Chinese Academy of Sciences, Lanzhou, 730000, People's Republic of China. E-mail: ydeng@licp.cas.cn

[c]Department of Electronic and Information Engineering, School of Information Science and Engineering, Shenyang University of Technology, Shenyang, 110870, People's Republic of China

† Electronic supplementary information (ESI) available. See DOI: 10.1039/c8ta02629g

HCl solution flowing over the graphene nano-channel using MD simulation. The research results confirmed that the coupling of the free charges that are present in graphene with the mobile surface charges (*i.e.*, adsorbed ions) is the main mechanism responsible for power generation from the flow, that is, the power generation is primarily caused by a net drift velocity of adsorbed Cl^- ions on the continuous graphene film surface. Meanwhile, they also drove the ~0.6 M HCl solution flowing over a ~30 × 16 μm^2 graphene film and experimentally measured a peak flow-induced voltage of ~30 mV.

In 2001, a flow-induced electric current was first experimentally obtained from metallic carbon nano-tubes immersed in liquids flowing along them;[8] subsequently, flow-induced voltages were also observed from flowing water, HCl solution, methanol, and glycerol on SWCNT bundles in 2003.[9] Subsequently, different experiments have been reported[4,10–20] at the micron scale, which revealed the actual causes of flow-induced voltage or electric current generation,[2,5,8,9,21,22] such as electron drag.[8] However, the liquids used in all the above-mentioned works are deionization water, inorganic HCl solution, organic methanol/ethanol aqueous solutions, *etc.* These common liquids are generally volatile, virose, and caustic, which limit their application in energy harvesting systems. Room temperature ionic liquids (RTILs) are environmentally friendly, healthy, safe, and highly thermostable because of which they have been widely investigated as novel solvents, electrolytes, and soft functional materials as liquids in liquid-flow-induced energy harvesting systems.[7,23,24] On the other hand, it is very difficult to experimentally observe the microscopic details on the nano-scale due to the limitations of the experimental equipment and increased technical complexity. Therefore, in our previous work,[25] a structure consisting of a nano-sized imidazolium-based RTIL droplet and monolayer graphene sheet with dimensions of 8.64 × 7.46 nm^2 was employed to explore the phenomenon of voltage generation using MD simulation. A flow-induced voltage of ~2.5 μV was obtained by accelerating this droplet along the monolayer graphene sheet.

In this study, flow-induced voltage is investigated by driving pure bulk RTIL 1-ethyl-3-methylimidazolium tetrafluoroborate ([Emim][BF_4]) flowing over a graphene nano-channel consisting of two parallel single-layered graphene sheets using MD simulation for the first time. Because the distance between two parallel single-layered graphene sheets and area of single-layered graphene directly affect the distribution of anions and cations in the adsorbed layer, considering the combined effect of anions and cations in the adsorbed layer on the free charge carrier of the graphene surfaces (interactions are 12.0 and 7.0 kJ mol^{-1} per cation/anion and graphene, respectively) and the characteristic of Coulomb's law, we have developed an advanced equation that can effectively and accurately calculate the flow-induced voltage of RTIL and graphene nano-channel system on the nano-scale. Based on our developed advanced equation, a maximal flow-induced voltage of 2.3 μV was obtained from such nano-scaled energy harvesting system; meanwhile, the mechanism of flow-induced voltage generation is revealed as the free charge carriers on the graphene nano-channel surface are dragged along pure bulk RTIL's direction of movement, thereby generating flow-induced voltage. A saturation of flow-induced voltage with increase of flow velocity is observed, and we attribute this saturation mechanism to the balance between the external driving force and viscous resistance arising from internal RTIL and graphene nano-channels. Moreover, the influence of the distance between two parallel single-layered graphene sheets of the graphene nano-channel, single-layered graphene area, system temperature (viscosity), and average flow velocity on the flow-induced voltage is also investigated.

2 Molecular models and simulation methods

2.1 Molecular models

In this study, the imidazolium-based RTIL [Emim][BF_4] flowing over a graphene nano-channel under acceleration to generate flow-induced voltage is studied by using MD simulation. Molecular structures of the cations and anions used are shown in Fig. 1. The energy harvesting mechanism was examined by simulating the RTIL to flow over the graphene nano-channel and observing the flow-induced voltage generation. Pure bulk RTILs comprise some ion pairs, initially stacked in a simple cubic structure, making use of the PACKMOL software,[26] where the initial structure of a single RTIL pair is derived from the Cambridge Crystallographic Data Centre (CCDC). For the MD simulation presented in this paper, the lengths of all the used cubic bulk RTIL droplets are 1, 2, 3, 4 and 5 nm. The numbers of [Emim][BF_4] ion pairs under different graphene areas and graphene nano-channel sizes are presented in Table 1. The graphene nano-channel consists of two single-layered graphene sheets with dimensions ranging from 1 to 25 nm^2. The graphene planes are flexible, but their centres of mass (COMs) are fixed to prevent the graphene from shifting under simulation. Fig. 2 shows the ensemble structure with the initial cubic bulk including 450

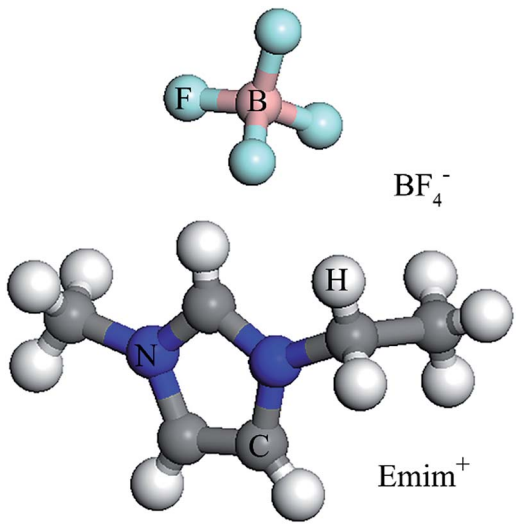

Fig. 1 Molecular structures of 1-ethyl-3-methylimidazolium ($Emim^+$) and tetrafluoroborate (BF_4^-).

Table 1 [Emim][BF_4] ion pairs under different graphene areas and nano-channel sizes

Size = 5 nm					
Area (nm^2)	1	4	9	16	25
Pairs (N)	18	72	162	288	450
Area = 25 nm^2					
Size (nm)	1	2	3	4	5
Pairs (N)	64	160	257	353	450

[Emim][BF_4] ion pairs obtained from a separate MD simulation, and the length of the side of the cubic bulk RTIL is 5 nm. The dimensions of the simulation box are set as $5.0 \times 5.0 \times 10.0$ nm^3 to avoid interactions with neighboring cells (z direction). The ensemble structure is the centre of the simulation box. Orthorhombic periodic boundary conditions (PBC) were applied to all the three directions of the simulated box during the entire simulation.

2.2 Simulation methods

All the MD simulations were carried out using the general purpose parallel MD simulation open-source package DL_POLY 4.08.[27] Intra- and intermolecular interactions were represented using a non-polarizable all-atom force field developed by Wang *et al.* with the functional form for potential energy U:[28,29]

$$\begin{aligned} U_{\text{total}} &= U_{\text{bonds}} + U_{\text{angles}} + U_{\text{dihedrals}} + U_{\text{nonbond}} \\ &= \sum_{\text{bonds}} K_r(r - r_0)^2 + \sum_{\text{angles}} K_\theta(\theta - \theta_0)^2 \\ &\quad + \sum_{\text{dihedrals}} \frac{K_\varphi}{2}[1 + \cos(n\phi - \gamma)] \\ &\quad + \sum_{i<j}\left\{4\varepsilon_{ij}\left[\left(\frac{\sigma_{ij}}{r_{ij}}\right)^{12} - \left(\frac{\sigma_{ij}}{r_{ij}}\right)^{6}\right] + \frac{q_i q_j}{4\pi\varepsilon_0\varepsilon_r r_{ij}}\right\} \end{aligned} \quad (1)$$

the first three terms represent bonded interactions, *i.e.*, bonds, angles, and dihedrals. The non-bonded interactions are described in the last term, including van der Waals (VDW, in the Lennard-Jones (LJ) 12-6 form) and coulombic interactions of atom-centred point charges. Electrostatic and VDW interactions are calculated only between the atoms in different molecules or for the atoms in the same molecule separated by at least three bonds. The VDW interaction parameters between different atoms are obtained from the Lorentz–Berthelot combining rules.[30] For the carbon atoms of the graphene nano-channel, the 12-6 LJ potential parameters are 0.4056 kJ mol^{-1} and 0.34 nm.[31] The Tersoff–Brenner covalent potential[32–34] that successfully describe the mechanical properties of carbon nano-tubes[35] is used to describe the interaction between the carbon atoms of the graphene sheet: the parameters are listed in Table 2.[34]

The Newton's equation of motion is integrated using a velocity Verlet algorithm with an integration time of 2.0 fs under the NVT ensemble. A Nosé–Hoover thermostat[36,37] with a relaxation time constant of 1.0 ps is applied to the system to maintain a desired constant temperature corresponding to the melting point of liquid of the respective system, and the simulation temperature ranges from 300 to 375 K for the studied RTILs. The initial velocities are randomly assigned to the atoms according to the system's temperature. The cutoff of the LJ and electrostatic interactions is taken as 1.5 nm. Long-range coulombic interactions are treated using the smooth particle mesh Ewald (PME) method.[38]

The initial pure bulk RTIL configurations are equilibrated at the appropriate temperature under the NPT ensemble until the experimental value of the liquid density is obtained and the total energy of the system converges to a constant (Fig. S1†). In the results presented below, the initial configurations are firstly equilibrated at $T = 1000$ K for 1 ns. The equilibrated configuration at this temperature is then cooled down sequentially to 300 K, with an interval of 100 K. At each temperature, the system is equilibrated with the NVT simulation for 1 ns. The obtained configuration at $T = 300$ K is then allowed to run for 10 ns to ensure a better equilibrium state. After equilibration, a series of acceleration values ranging from 0.001 to 0.2 nm ps^{-2} imposed only along the y direction are applied on the pure bulk RTIL to collect corresponding data taken every 1000 time steps in the next 10 ns. Similar simulation procedures are performed with regard to temperatures above 300 K. After the simulation, the physical properties are characterized using the DL_POLY analysis tools, and the structures are visualized with a molecular graphics software named visual molecular dynamics (VMD).[39]

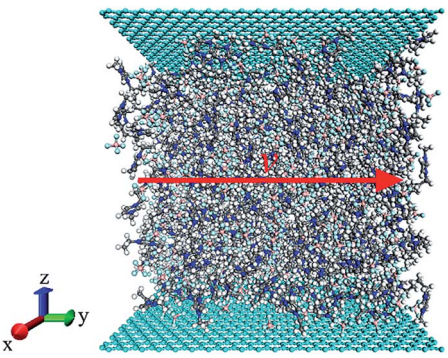

Fig. 2 Initial structure of the ensemble including cubic bulk RTIL droplets and graphene nano-channels.

Table 2 Parameters in Tersoff potential for graphene

Parameter	Carbon
A (kJ)	1.3446×10^5
B (kJ)	3.3451×10^5
λ (nm^{-1})	34.879
μ (nm^{-1})	22.119
β	1.5724×10^{-7}
n	7.2571×10^{-1}
c	3.8049×10^4
d	4.3840
h	-5.7058×10^{-1}
R (nm)	0.18
S (nm)	0.21
χ_{C-C}	1.0

3 Results and discussion

When the simulation systems reach equilibrium, the VDW interactions between the cations/anions and graphene nano-channel compel the cations and anions to aggregate on the graphene surface, forming a stronger adsorbed layer; this can be visually seen from Fig. 3a. By analysing the mean number densities of anions and cations obtained from the position of their COMs in the direction perpendicular to the graphene surfaces (z direction), we find that these densities exhibit larger fluctuations, reaching maximal values near the graphene surfaces (Fig. 3b); this confirms the formation of a strongly adsorbed layer near the graphene surfaces. Nevertheless, for the direction parallel to the graphene surfaces (x and y directions), the mean number densities of cations and anions fluctuates across a fixed value, and no distinct layers occur close to the graphene surfaces (Fig. S2†). Therefore, only the influence of ion distribution along the z direction is considered when we calculated the flow-induced voltage in this study, the ion distributions of RTILs in the x and y directions are not considered.

Under acceleration, the anions and cations of bulk RTILs move along the graphene nano-channel. On the basis of the simulation results, we estimate the accumulated displacements of anions and cations in each direction and find the accumulated displacements in the x and z directions are much less than that in the y direction, which indicates that when an external force is applied along the y direction, the cations and anions are driven along the graphene nano-channel in the y direction. Fig. 4 shows the accumulated displacement of anions and cations inside the graphene nano-channel (Fig. 3a). It is evident that the slope of the accumulated displacement curves of the anions and cations increases with time, tending toward a fixed value. This means the average flow velocity of the anions and cations nonlinearly increases to saturation with time, which is consistent with previous research results.[3,4,25] As the average flow velocity is eventually almost a constant, the effect of self-consistent voltage generation can be neglected.[3,4] According to the accumulated displacements in the y direction, we calculate the average flow velocities of anions and cations in the flow direction under different applied acceleration values, as shown in Fig. 5.

Fig. 5 depicts that the average flow velocities of anions and cations have a nonlinear increase with time, ultimately reaching a level of saturation. Under applied acceleration, the anions and cations move along the direction of external force in the graphene nano-channel and the flow velocity gradually increases. Generally, constant acceleration applied to anions and cations can make their velocities continuously increase linearly, and the saturation phenomenon is not observed. However, the velocity of anions and cations moving along the graphene nano-channel exhibits an obvious saturation trend under applied acceleration; this saturation can be attributed to the viscous resistance arising from internal RTILs and graphene nano-channels. It is well known that the viscous resistance is directly proportional to the moving velocity of the object in liquid. When the anions and

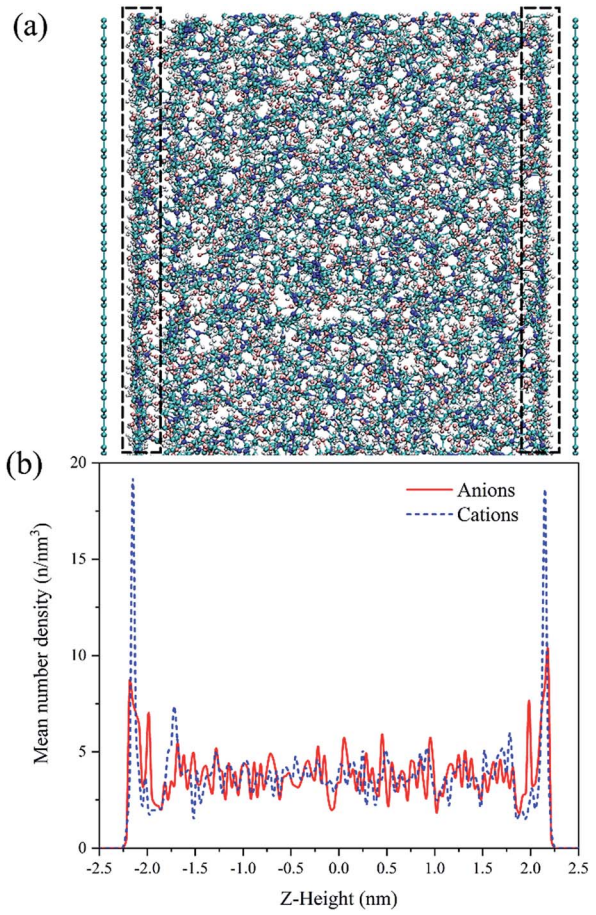

Fig. 3 (a) Equilibrium structure of the RTILs [Emim][BF_4] and graphene nano-channel, (b) mean number densities of anions and cations in the z direction: red solid line denotes anions; blue dashed line denotes cations.

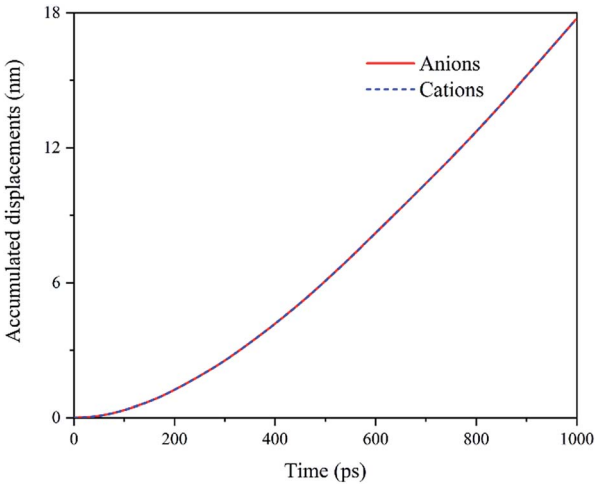

Fig. 4 Accumulated displacements of anions and cations inside the graphene nano-channel at applied acceleration of 0.15 nm ps^{-2}, where the system temperature is 300 K and the size of graphene nano-channel is 5 nm.

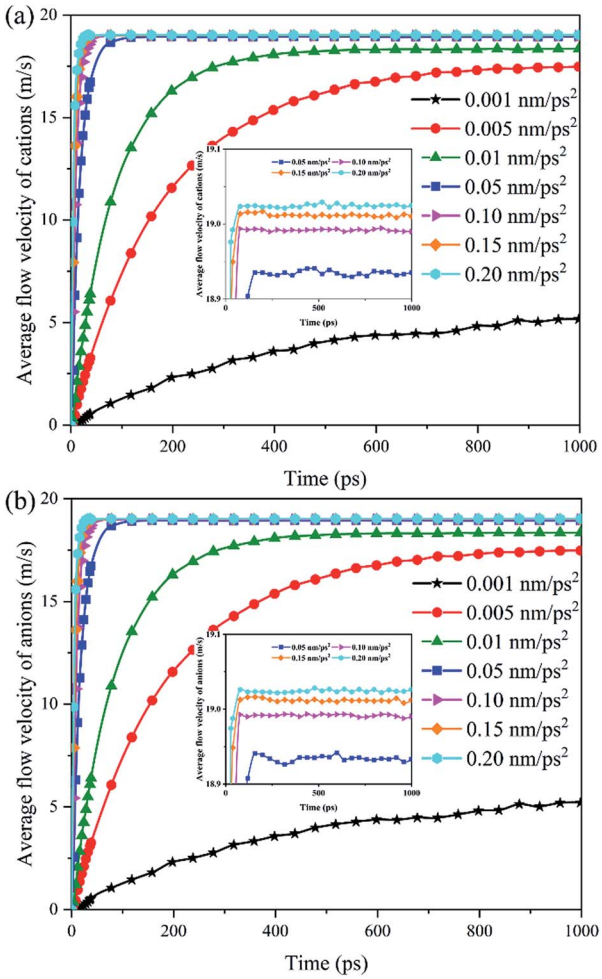

Fig. 5 Average flow velocity of cations $Emim^+$ in (a) and anions BF_4^- in (b), varying with time under different applied acceleration values at 300 K.

cations flow over the graphene nano-channel under acceleration, the viscous resistance gradually increases with the velocity of anions and cations until the viscous resistance is equal to the external driving force developed by this acceleration. At this time, the restriction coming from the viscous resistance makes the velocity of anions and cations no longer increase, tending toward saturation. Fig. 5 also demonstrates that larger acceleration can make the velocity of anions and cations reach a threshold value in a short period of time, but the ultimate velocity of the anions and cations is basically the same under different acceleration values.

Under steady flow, the anions and cations move along the graphene nano-channel and then drag the free charge carriers drifting along the graphene surfaces due to their strong interactions with the adjacent anions/cations and graphene. These carriers drifting along the graphene surfaces can generate a flow-induced voltage. As shown in previous works, when the HCl solution is moved along CNTs or graphene, only the anions are involved in the generation of flow-induced voltage and the cations are not considered due to their weaker interactions with the CNTs or graphene.[3,4] The flow-induced voltage was generally estimated by[5]

$$V = RI = R\sigma eLv \tag{2}$$

where $R = \rho L/S$ is the graphene sheet resistance; ρ, resistivity of graphene of 10^{-8} Ωm; L and S, contact length and contact area of the droplet with graphene sheet, respectively; σ, range of the average free charge carrier density of graphene and is within 10^{19}–10^{20} m^{-2}; e, electronic charge of 1.6×10^{-19} C; and v, average drifting velocities of anions (Cl^-).

For the anions and cations of RTILs moving along the graphene surface, the VDW interaction between these ions and graphene compels them to accumulate on the graphene surface, forming a strong adsorption layer owing to the complex structures and larger volumes of cations and anions in RTILs. Therefore, the effect of anions and cations should be entirely taken into consideration when calculating flow-induced voltages. This is because the anions and cations form the adsorbed layers together near the graphene nano-channel surfaces (Fig. 3) and contribute toward the generation of flow-induced voltage. That is, the anions and cations in the adsorbed layer together drag the free charge carrier on the graphene surface drifting along the force direction, and all of them contribute toward the generation of flow-induced voltage. Although the cations and anions in the adsorbed layers are drifting in the same direction under the applied acceleration, the drifting anions can induce a current in the opposite direction of anions' and cations' movement, which cancels out or reduces the current flow resulting from the drifting of cations along the direction of movement. Moreover, the strengths of coulombic interactions between the anions/cations and graphene are directly proportional to the charge and inversely proportional to the square of the distance. Therefore, based on the aforementioned results and taking the combined effect of anions and cations in the adsorbed layer into consideration (the interactions are 12.0 and 7.0 kJ mol^{-1} per cation/anion and graphene, respectively), we developed the traditional equation to calculate the flow-induced voltage as follows:

$$V = RI = R\sigma eL\left(v^+ - \frac{\left|\int_a^b \frac{1}{z^2}\rho^-(z)\mathrm{d}z\right|}{\left|\int_a^b \frac{1}{z^2}\rho^+(z)\mathrm{d}z\right|}v^-\right) \tag{3}$$

where v^+ and v^- are the average drifting velocities of cations and anions, respectively. Further, ρ^+ and ρ^- are the charge densities of cations and anions along the coordinate perpendicular to the graphene surface, respectively. $\int_a^b \frac{1}{z^2}\rho^-(z)\mathrm{d}z$ represents the integral of the modified anions charge density $\frac{1}{z^2}\rho^-(z)$ from a to b, which is the range of the adsorbed layer (Fig. 6); this term is based on the combined effect of anions and cations in the adsorbed layer on the free charge carrier of the graphene surfaces. The coefficient $\frac{1}{z^2}$ is based on the coulombic interactions strength between the anions/cations and graphene, which

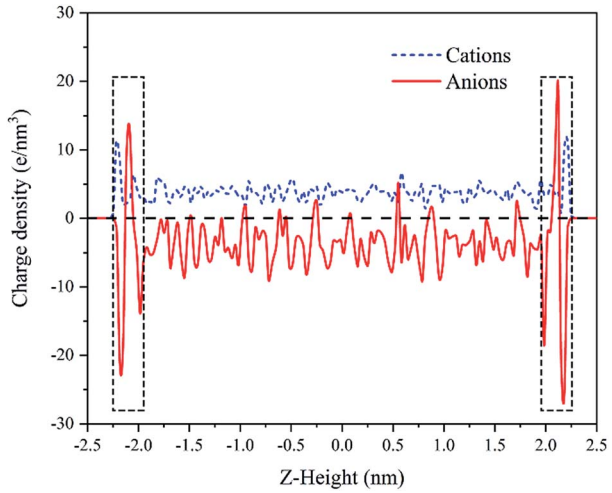

Fig. 6 Charge density of anions and cations in the z direction: red solid line denotes the anions and blue dashed line denotes the cations.

is inversely proportional to the square of the distance. Likely, the $\int_a^b \frac{1}{z^2}\rho^+(z)\mathrm{d}z$ in the denominator represents the integral of the modified cations' charge density $\frac{1}{z^2}\rho^+(z)$ from a to b.

According to our developed equation, we estimate the flow-induced voltage for different average charge carrier densities of graphene, and the results are presented in Fig. 7. From this figure, it is evident that the flow-induced voltages of about 0.21–2.1 μV are generated from relatively small dimensioned models of nano-sized pure bulk RTIL [Emim][BF_4] moving along the graphene nano-channel at 300 K in our simulations. These values are very close to the flow-induced voltage values generated from a nano-sized RTIL droplet flowing over monolayer graphene,[25] while the slight difference in the flow-induced voltages rising from these two different energy harvesting systems can be attributed to the additional viscous resistance coming from the graphene nano-channel imposing on pure bulk RTILs. Similarly, the saturation phenomenon of the flow-induced voltage is also observed (Fig. 7), which is qualitatively similar to previous results[3,4,25] and caused by the force balance between the external applied force and the internal viscous resistance arising from internal RTILs and the graphene nano-channel. In a previous work,[4] about 85 nW of output power was generated from ~0.6 M HCl solution at the rate of ~0.01 m s^{-1} flowing over a graphene film with dimension of ~30 × 16 μm, which equates to a power per unit area of ~175 W m^{-2}. If the energy harvesting systems have the same size, pure bulk RTILs flowing over graphene nano-channels can produce up to 88 nW of output power, as per our simulations, which equates to a power per unit area of ~183 W m^{-2}. This shows an improvement of about 5% in the power per unit area when compared to that obtained from ~0.6 M HCl solution flowing over a graphene nano-channel.

Nano-fluidic behaviour is greatly dependent on the temperature because temperature directly affects the viscosity of nano-

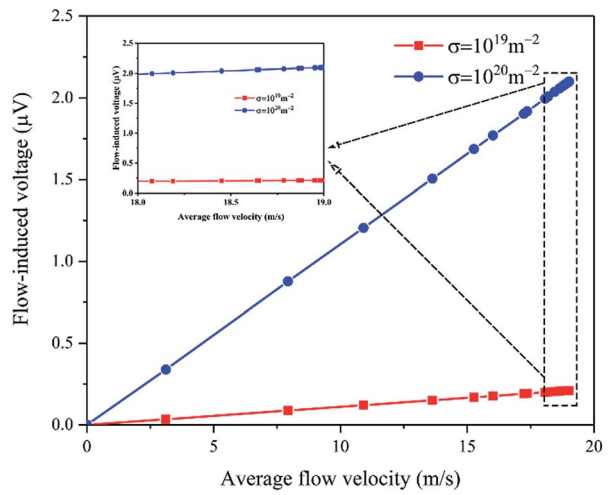

Fig. 7 Flow-induced voltage as a function of the average flow velocity under applied acceleration of 0.15 nm ps^{-2} at 300 K. The lines are drawn only for guidance purposes.

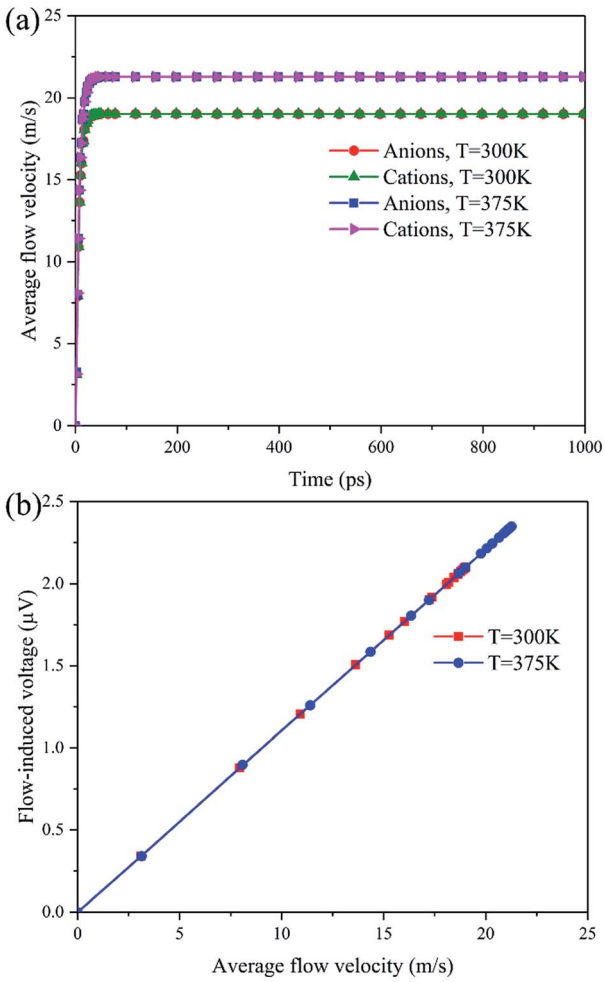

Fig. 8 Average flow velocity of anions and cations at T = 300/375 K in (a) and flow-induced voltage as a function of the average flow velocity under applied acceleration of 0.15 nm ps^{-2} at T = 300/375 K in (b). The lines are drawn only for guidance purposes.

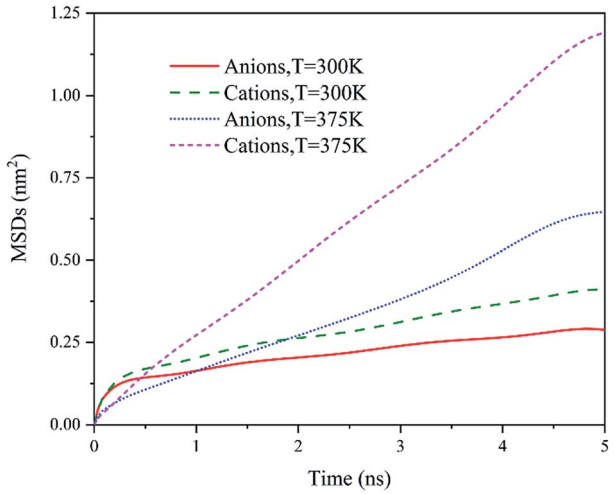

Fig. 9 MSDs of cations and anions for RTILs [Emim][BF_4] at $T = 300$ and 375 K.

confined liquids.[7] Therefore, the influence of temperature on the flow-induced voltage is investigated at $T = 300$ and 375 K. Fig. 8a shows that the average flow velocities of cations and anions at $T = 375$ K exhibit an obvious increase when compared with the average flow velocities of cations and anions at $T = 300$ K. With the increase in temperature, the viscosity of RTILs confined in the graphene nano-channel decreases. Consequently, the effect of viscous resistance arising from internal RTILs on cations and anions is impaired and the ions move at larger velocities because of good fluidity and mobility. The mobilities of cations and anions can be seen from the mean square displacements (MSDs)[30] derived from the MD simulation runs. Fig. 9 intuitively illustrates that the MSDs of cations and anions at $T = 375$ K exhibit a clear increase when compared with those at $T = 300$ K. This increase indicates that the cations and anions can more easily come out of their initial positions and achieve larger velocities; this is consistent with the average flow velocity presented in Fig. 8a. Likewise, we estimate the flow-induced voltage on the basis of the average flow velocities of cations and anions at $T = 375$ K, as shown in Fig. 8b. From Fig. 8b, it is evident that the flow-induced voltage has a significant increase at $T = 375$ K, and a flow-induced voltage of 2.35 μV has been obtained from flowing RTILs in the graphene nano-channel. It is noteworthy that the flow-induced voltage tends to be saturated as the average flow velocity reaches the level of saturation caused by the constraint arising from the viscous resistance.

The distance between two parallel single-layered graphene sheets of the graphene nano-channel clearly affects the degree of nano-confinement, and therefore, the average flow velocities of cations and anions. Following a similar procedure, the influence of the distance between two parallel single-layered graphene sheets of the graphene nano-channel on the flow-induced voltage is investigated by employing different graphene nano-channel sizes such as 1, 2, 3, 4, and 5 nm. Fig. 10 shows that the average flow velocities of cations and anions increase as the graphene nano-channel size increases,

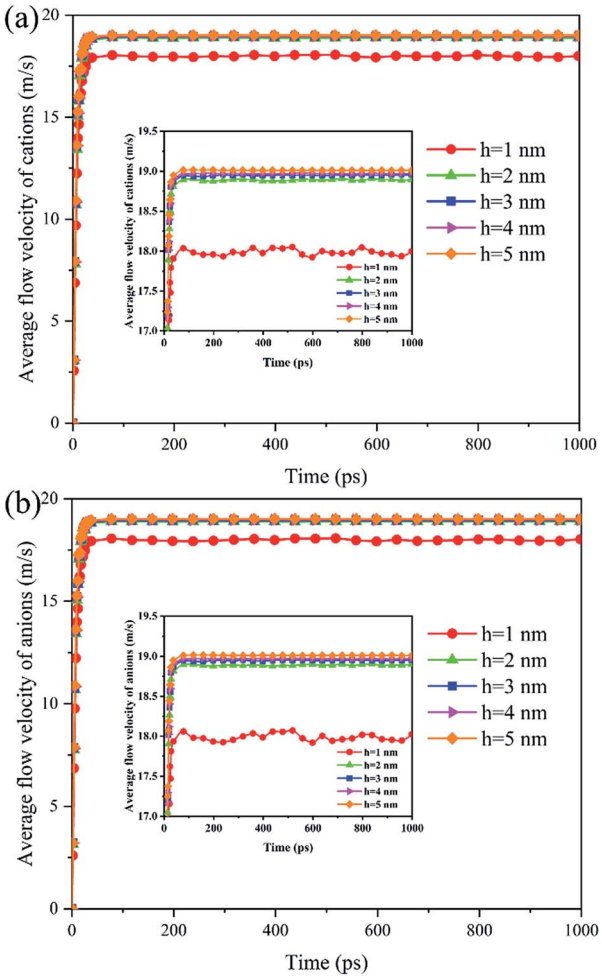

Fig. 10 Average flow velocity of cations $Emim^+$ in (a) and anions BF_4^- in (b), varying with time under applied acceleration of 0.15 nm ps^{-2} at 300 K.

eventually tending toward saturation. An increase in the distance between the two parallel graphene sheets in the graphene nano-channel may decrease the number of collisions per unit volume, and also, increase the fraction of ions that are away from the surface and increase the flow velocities.[7,40] On the other hand, an increase in the graphene nano-channel size weakens the interaction between graphene and cations/anions and increases the flow velocity of cations and anions; this is quantified by the MD simulation results using the radial distribution function (RDF) plotted in Fig. 11. From this figure, we can determine that the number of cations and anions decreases as the graphene nano-channel size increases, revealing that the interaction between graphene and cations/anions is weakened with an increase in the distance between two parallel single-layered graphene sheets of the graphene nano-channel. Therefore, the viscous resistance of the graphene nano-channel toward the cations and anions of RTILs is weakened, too, and the cations and anions move with larger flow velocities. Nevertheless, the average flow velocity does not continuously increase as the graphene nano-channel size increases because the viscous resistance arising from the

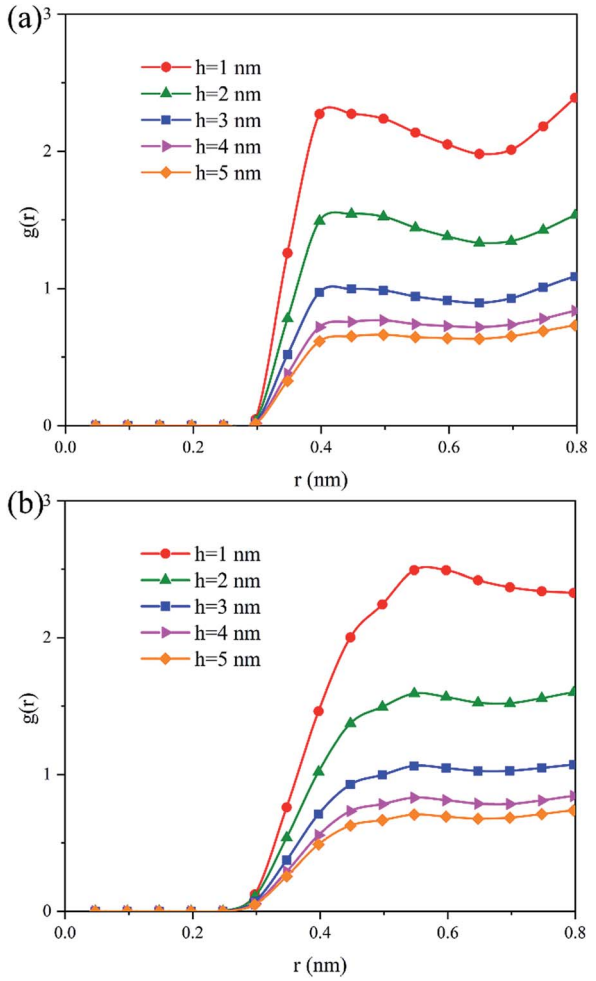

Fig. 11 COM RDFs for (a) cations and (b) anions around the carbon atoms of a graphene nano-channel.

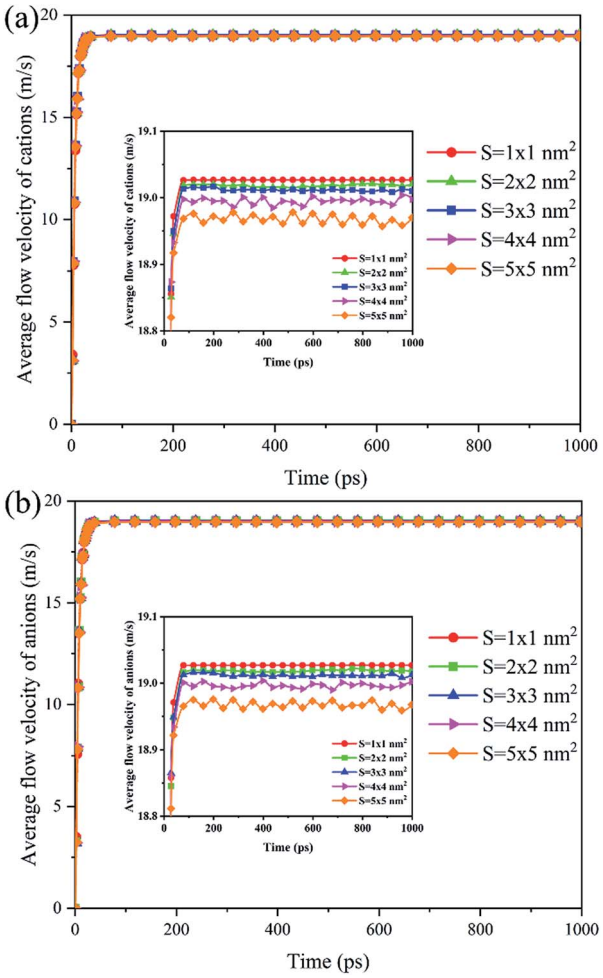

Fig. 13 Average flow velocity of cations $Emim^+$ in (a) and anions BF_4^- in (b), varying with time under applied acceleration of 0.15 nm ps^{-2} at 300 K.

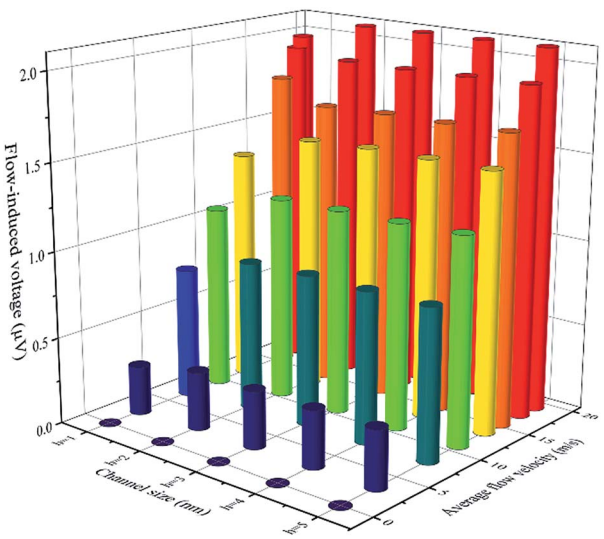

Fig. 12 Flow-induced voltage as a function of the average flow velocity under different graphene nano-channel sizes: the applied acceleration is 0.15 nm ps^{-2} and the temperature is 300 K.

internal RTILs plays a dominant role in larger graphene nano-channel size and constrains the increase in the average flow velocities. When the viscous resistance arising from the internal RTILs is balanced by the external driving force developed by acceleration, the average flow velocity no longer increases and tends to become saturated. Due to the increase in the average flow velocities of cations and anions toward saturation with an increase in the graphene nano-channel size, according to our developed eqn (3), the flow-induced voltages also increase as the graphene nano-channel size increases, tending toward saturation, as shown in Fig. 12.

Additionally, the generation of the flow-induced voltage is dependent on the area of single-layered graphene in a graphene nano-channel. The MD simulations performed for single-layered graphene with areas of 1, 4, 9, 16, and 25 nm^2 would allow for the interference of the effect of single-layered graphene area on the flow-induced voltage. The average flow velocities of cations and anions are presented in Fig. 13, which show that the average flow velocities of cations and anions decrease as the single-layered graphene area increases, eventually tending toward saturation. With increasing single-layered

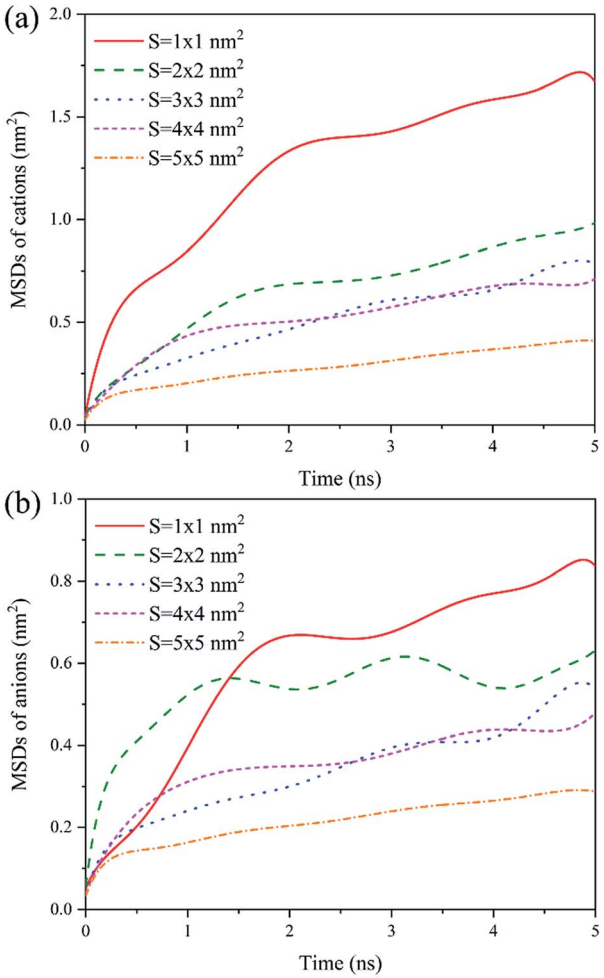

Fig. 14 MSDs of cations and anions for RTILs [Emim][BF_4] in different single-layered areas at $T = 300$ K.

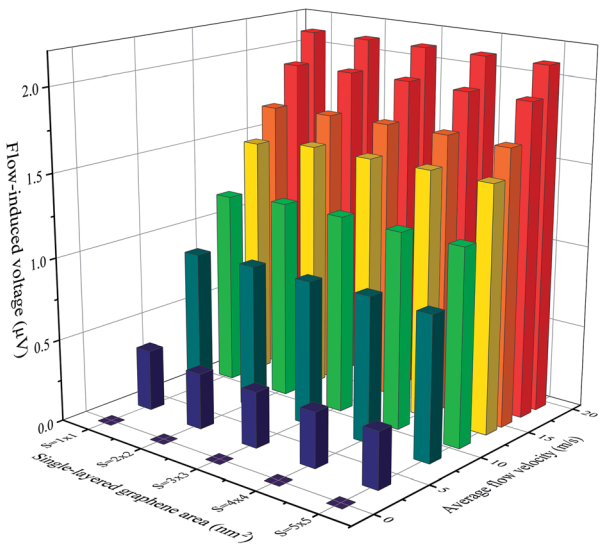

Fig. 15 Flow-induced voltage as a function of the average flow velocity in different single-layered graphene areas; the applied acceleration is 0.15 nm ps^{-2} and the temperature is 300 K.

graphene area, the contact area of RTILs and graphene nano-channel also increases. Therefore, the viscous resistance of the graphene nano-channel toward cations and anions of RTILs is enhanced, too, which is imposed on the cations and anions of RTILs, thereby reducing the fluidity of RTILs and mobilities of cations and anions. The fluidity of RTILs and mobilities of cations and anions are quantified by the MSDs of cations and anions for different single-layered graphene areas, as shown in Fig. 14. From this figure, it is evident that the MSDs of cations and anions show larger values and decrease with an increase in the single-layered graphene area; this indicates that the fluidity of RTILs and mobilities of cations and anions reduce and the cations and anions in a smaller area of single-layered graphene can achieve larger flow velocities. Likewise, the average flow velocity does not continuously increase as the area of single-layered graphene decreases owing to the viscous resistance arising from the internal RTILs and graphene nano-channel, which hinders the increase in the average flow velocities. On the basis of our developed eqn (3), we calculated the flow-induced voltage in different single-layered graphene areas, as shown in Fig. 15.

4 Conclusions

In summary, flow-induced voltage is investigated by driving pure bulk RTIL [Emim][BF_4] flowing over a graphene nano-channel consisting of two parallel single-layered graphene sheets using MD simulations for the first time. Considering the combined effect of anions and cations in the adsorbed layer on the free charge carriers of the graphene surfaces and the characteristic of Coulomb's law, we develop an advanced equation that can effectively and accurately calculate the flow-induced voltage of this RTIL and graphene nano-channel system on the nano-scale. According to our developed equation, a maximal flow-induced voltage of 2.3 μV is obtained from such a nano-scaled system because the free charge carrier on the graphene channel surfaces is dragged along the pure bulk RTIL's direction of movement. A saturation of flow-induced voltage with an increase in the flow velocity is observed, and this saturation can be attributed toward the balance between the external driving force and viscous resistance arising from internal RTIL and graphene nano-channel. Excitingly and feasibly, the power per unit area exhibits a 5% improvement when compared to ~0.6 M HCl solution flowing over the graphene nano-channel consisting of two parallel single-layered graphene planes (4.26 × 2.46 nm^2). Further analysis shows that the flow-induced voltages gradually increase toward saturation from 1.9 to 2.1 μV or decrease from 2.3 to 2.1 μV when the distance between the two parallel single-layered graphene or the area of a single layer of the graphene nano-channel increases from 1 to 5 nm or from 1 to 25 nm^2, respectively. Moreover, studies have shown that the flow-induced voltage increases with the applied acceleration (average flow velocity) and temperature (viscosity), and these trends are attributable to the competition between the external driving force developed by the acceleration and the viscous resistance arising from internal RTIL and graphene nano-channel. We anticipate that the study presented here provides

a deeper understanding of energy harvesting on the nano-scale and can promote the development and application of NEMSs based on RTILs and graphene.

Conflicts of interest

There are no conflicts to declare.

Acknowledgements

The authors acknowledge the financial support of this work from the National Key Research and Development Program of China (2017YFA0403101) and the Fundamental Research Funds for the Central Universities (No. lzujbky-2018-it62).

References

1 Z. L. Wang, *Adv. Mater.*, 2012, **24**, 280–285.
2 Q. Yuan and Y. P. Zhao, *J. Am. Chem. Soc.*, 2009, **131**, 6374–6376.
3 B. Xu and X. Chen, *Phys. Chem. Chem. Phys.*, 2013, **15**, 1164–1168.
4 P. Dhiman, F. Yavari, X. Mi, H. Gullapalli, Y. Shi, P. M. Ajayan and N. Koratkar, *Nano Lett.*, 2011, **11**, 3123–3127.
5 B. N. J. Persson, U. Tartaglino, E. Tosatti and H. Ueba, *Phys. Rev. B: Condens. Matter Mater. Phys.*, 2004, **69**, 235410.
6 B. Radha, A. Esfandiar, F. C. Wang, A. P. Rooney, K. Gopinadhan, A. Keerthi, A. Mishchenko, A. Janardanan, P. Blake, L. Fumagalli, M. Lozada-Hidalgo, S. Garaj, S. J. Haigh, I. V. Grigorieva, H. A. Wu and A. K. Geim, *Nature*, 2016, **538**, 222–225.
7 S. Zhang, J. Zhang, Y. Zhang and Y. Deng, *Chem. Rev.*, 2017, **117**, 6755–6833.
8 P. Kral and M. Shapiro, *Phys. Rev. Lett.*, 2001, **86**, 131–134.
9 S. Ghosh, A. K. Sood and N. Kumar, *Science*, 2003, **299**, 1042–1044.
10 S. Ghosh, A. Sood, S. Ramaswamy and N. Kumar, *Phys. Rev. B: Condens. Matter Mater. Phys.*, 2004, **70**, 205423.
11 S. H. Lee, D. Kim, S. Kim and C. S. Han, *Appl. Phys. Lett.*, 2011, **99**, 104103.
12 J. Yin, Z. Zhang, X. Li, J. Zhou and W. Guo, *Nano Lett.*, 2012, **12**, 1736–1741.
13 S. H. Lee, Y. Jung, S. Kim and C. S. Han, *Appl. Phys. Lett.*, 2013, **102**, 063116.
14 S. H. Lee, Y. B. Kang, W. Jung, Y. Jung, S. Kim and H. M. Noh, *Nanoscale Res. Lett.*, 2013, **8**, 487.
15 W. Huang, G. Wang, F. Gao, Z. Qiao, G. Wang, M. Chen, Y. Deng, L. Tao, Y. Zhao, X. Fan and L. Sun, *J. Phys. Chem. C*, 2014, **118**, 8783–8787.
16 W. Huang, G. Wang, F. Gao, Z. Qiao, G. Wang, L. Tao, M. Chen, F. Yu, H. Yang and L. Sun, *Nanoscale*, 2014, **6**, 3921–3924.
17 J. Yin, X. Li, J. Yu, Z. Zhang, J. Zhou and W. Guo, *Nat. Nanotechnol.*, 2014, **9**, 378–383.
18 J. Yin, Z. Zhang, X. Li, J. Yu, J. Zhou, Y. Chen and W. Guo, *Nat. Commun.*, 2014, **5**, 3582.
19 Y. He, J. Lao, T. Yang, X. Li, X. Zang, X. Li, M. Zhu, Q. Chen, M. Zhong and H. Zhu, *Appl. Phys. Lett.*, 2015, **107**, 081605.
20 H. Zhong, J. Xia, F. Wang, H. Chen, H. Wu and S. Lin, *Adv. Funct. Mater.*, 2017, **27**, 1604226.
21 A. E. Cohen, *Science*, 2003, **300**, 1235–1236.
22 Y. C. Zhao, L. Song, K. Deng, Z. Liu, Z. X. Zhang, Y. L. Yang, C. Wang, H. F. Yang, A. Z. Jin, Q. Luo, C. Z. Gu, S. S. Xie and L. F. Sun, *Adv. Mater.*, 2008, **20**, 1772–1776.
23 S. Zhang, Q. Zhang, Y. Zhang, Z. Chen, M. Watanabe and Y. Deng, *Prog. Mater. Sci.*, 2016, **77**, 80–124.
24 Y. Guan, Q. Shao, W. Chen, S. Liu, X. Zhang and Y. Deng, *J. Phys. Chem. C*, 2017, **121**, 23716–23726.
25 Q. Shao, J. Jia, Y. Guan, X. He and X. Zhang, *J. Chem. Phys.*, 2016, **144**, 124703.
26 L. Martínez, R. Andrade, E. G. Birgin and J. M. Martínez, *J. Comput. Chem.*, 2009, **30**, 2157–2164.
27 I. T. Todorov, W. Smith, K. Trachenko and M. T. Dove, *J. Mater. Chem.*, 2006, **16**, 1911–1918.
28 W. D. Cornell, P. Cieplak, C. I. Bayly, I. R. Gould, K. M. Merz, D. M. Ferguson, D. C. Spellmeyer, T. Fox, J. W. Caldwell and P. A. Kollman, *J. Am. Chem. Soc.*, 1995, **117**, 5179–5197.
29 Z. Liu, S. Huang and W. Wang, *J. Phys. Chem. B*, 2004, **108**, 12978–12989.
30 M. P. Allen and D. J. Tildesley, *Computer simulation of liquids*, Oxford university press, 1989.
31 M. A. Moller, D. J. Tildesley, K. S. Kim and N. Quirke, *J. Chem. Phys.*, 1991, **94**, 8390–8401.
32 J. Tersoff, *Phys. Rev. Lett.*, 1988, **61**, 2879–2882.
33 J. Tersoff, *Phys. Rev. B: Condens. Matter Mater. Phys.*, 1989, **39**, 5566–5568.
34 W. C. D. Cheong and L. C. Zhang, *Nanotechnology*, 2000, **11**, 173.
35 B. Faria, N. Silvestre and J. N. Canongia Lopes, *Compos. Sci. Technol.*, 2011, **71**, 1811–1818.
36 S. Nosé, *J. Chem. Phys.*, 1984, **81**, 511–519.
37 W. G. Hoover, *Phys. Rev. A: At., Mol., Opt. Phys.*, 1985, **31**, 1695–1697.
38 U. Essmann, L. Perera, M. L. Berkowitz, T. Darden, H. Lee and L. G. Pedersen, *J. Chem. Phys.*, 1995, **103**, 8577–8593.
39 W. Humphrey, A. Dalke and K. Schulten, *J. Mol. Graphics*, 1996, **14**, 33–38.
40 N. N. Rajput, J. Monk, R. Singh and F. R. Hung, *J. Phys. Chem. C*, 2012, **116**, 5169–5181.

